Article

Not peer-reviewed version

DAPEG-Modified Analogs of Human Cathelicidin LL-37: Enhanced Proteolytic Stability and Selective Modulation of Neutrophil Degranulation

Wiktoria Rejmak , Katarzyna Bury , Marta Bauer , Wojciech Kamysz , Magdalena Wysocka , Adam Lesner *

Posted Date: 1 June 2026

doi: 10.20944/preprints202606.0060.v1

Keywords: cathelicidin LL-37; antimicrobial peptide; DAPEG; 2,3-diaminopropionic acid; proteinase 3; myeloperoxidase; PAD citrullination; solid-phase peptide synthesis; neutrophil degranulation; HL-60

 doi:10.20944/preprints202606.0060.v1

Article

DAPEG-Modified Analogs of Human Cathelicidin LL-37: Enhanced Proteolytic Stability and Selective Modulation of Neutrophil Degranulation

Wiktoria Rejmak [1], Katarzyna Bury [2], Marta Bauer [3], Wojciech Kamysz [3], Magdalena Wysocka [1] and Adam Lesner [1,*]

[1] Department of Environmental Technology, Laboratory of Biochemical Analytics and Nanodiagnostics, Faculty of Chemistry, University of Gdańsk, Wita Stwosza 63, 80-308 Gdańsk, Poland

[2] Intercollegiate Faculty of Biotechnology, University of Gdańsk and Medical University of Gdańsk, 80-307 Gdańsk, Poland

[3] Faculty of Pharmacy, Medical University of Gdańsk, Al. Gen. J. Hallera 107, 80-416 Gdańsk, Poland

* Correspondence: adam.lesner@ug.edu.pl; Tel.: +48-58-523-50-95

Abstract

The human cathelicidin LL-37 (37 amino acids; net charge +6) combines broad-spectrum antimicrobial activity with extensive immunomodulatory function, but its therapeutic exploitation is limited by rapid proteolytic degradation and post-translational inactivation through PAD-mediated citrullination of its arginine residues. We synthesized six analogs of LL-37 in which all five arginine residues (positions 7, 19, 23, 29, 34), all six lysine residues (positions 8, 10, 12, 15, 18, 25) or three isoleucine residues (positions 13, 20, 24) were replaced with the non-proteinogenic amino acid 2,3-diaminopropionic acid (Dap) functionalized on its side chain with either a one- or two-unit oxa-acid spacer (DAPEG building blocks). All compounds were obtained by Fmoc/tBu solid-phase peptide synthesis. Mass spectrometry, UPLC and circular dichroism confirmed identity, purity and partial retention of α-helical secondary structure. Proteolytic stability against human proteinase 3 was 5.7-fold increased for Dap(GO1)$^{[7,19,23,29,34]}$LL-37 relative to native LL-37; both arginine-substituted analogs showed delayed citrullination by PAD2 and PAD4, with the two-oxa-unit Dap(GO2)$^{[7,19,23,29,34]}$LL-37 conferring the greatest resistance. All analogs retained DNA binding by qualitative criteria, though DLS revealed reduced complex compaction for lysine-substituted analogs. All six DAPEG analogs lost the direct antibacterial activity of native LL-37 against reference Gram-positive and Gram-negative strains. None of the compounds was cytotoxic at 1–10 μM to HDFa, HB2, HL-60 or differentiated HL-60 cells. In differentiated HL-60 cells the lysine-substituted Dap(O1)$^{[8,10,12,15,18,25]}$LL-37 and Dap(O2)$^{[8,10,12,15,18,25]}$LL-37 analogs strongly suppressed LPS-induced secretion of both proteinase 3 and myeloperoxidase from azurophilic primary granules (~37-fold reduction of MPO at 1 h and 23–142-fold reduction at 24 h relative to LL-37 + LPS; all $p < 0.001$ by Sidak post-hoc) — a concordant two-marker signature of genuine inhibition of neutrophil degranulation. Isoleucine-substituted Dap(MO1)$^{[13,20,24]}$LL-37 and Dap(MO2)$^{[13,20,24]}$LL-37 analogs showed significant partial suppression of MPO secretion at both time points ($p < 0.001$ at 24 h); arginine-substituted analogs exhibited a biphasic phenotype, activating release at 1 h comparably to LL-37 but significantly reducing MPO at 24 h ($p < 0.05$). The DAPEG framework thus reprofiles the LL-37 scaffold from microbicidal toward selective immunomodulatory function, with the lysine-substituted analogs emerging as the most pharmacologically novel anti-inflammatory candidates.

Keywords: cathelicidin LL-37; antimicrobial peptide; DAPEG; 2,3-diaminopropionic acid; proteinase 3; myeloperoxidase; PAD citrullination; solid-phase peptide synthesis; neutrophil degranulation; HL-60

 doi:10.20944/preprints202606.0060.v1

1. Introduction

LL-37 is the only cathelicidin family member identified in humans [1]. It is generated by proteolytic processing of the precursor hCAP-18 by proteinase 3 in neutrophils and by kallikreins in epithelial cells [2]. The mature peptide — LLGDFFRKSKEKIGKEFKRIVQRIKDFLRNLVPRTES — carries a net positive charge of +6 at physiological pH and adopts an amphipathic α-helix on contact with anionic phospholipid bilayers [3,4], producing membrane disruption through carpet/toroidal-pore mechanisms with broad-spectrum activity against Gram-positive and Gram-negative bacteria, fungi and enveloped viruses [5,6,15]. Beyond direct microbicidal activity, LL-37 functions as a multipotent immunomodulator: it chemoattracts neutrophils, monocytes and T cells through the formyl peptide receptor 2 (FPR2; also known as FPRL1) [7]; delays constitutive neutrophil apoptosis [8]; modulates TLR4 signaling [22,23]; and contributes to neutrophil extracellular trap (NET) formation and degranulation [9,24,28].

Two major obstacles limit clinical translation of LL-37. First, the peptide is rapidly degraded by host and bacterial proteases, with a biological half-life in serum and wound fluid of minutes to hours [2,13,15]. Second, peptidylarginine deiminases (PAD2, PAD4), activated by intracellular calcium during NETosis [9], citrullinate the arginine side chains of LL-37, eliminating its positive charge and abolishing membrane-disrupting activity while conferring autoantigenic properties implicated in psoriasis and systemic lupus erythematosus [10,11,30]. Multiple chemical strategies — selective substitution [12], hydrocarbon stapling [16], N-methylation [17], engineered SAAP-148 [14] and PEGylation [13] — have been pursued, with varying success in balancing stability, activity and selectivity.

An alternative strategy that has emerged from the work of Wysocka and colleagues uses building blocks based on 2,3-diaminopropionic acid (Dap) modified on the side-chain amino group with a functionalized oxa-acid: the DAPEG framework [18–21]. These bifunctional monomers are fully compatible with Fmoc solid-phase peptide synthesis: a guanidinium-bearing oxa-acid converts Dap into an Arg mimetic, while an amino-bearing oxa-acid converts Dap into a Lys mimetic. The hydrophilic oxa-spacer increases aqueous solubility, suppresses aggregation and provides PEG-like steric shielding [18,19]. DAPEG polymers have recently been shown to penetrate mammalian cell membranes without cytotoxicity and to mediate transfection [20,21], establishing the platform as biocompatible.

Here we report the synthesis and biological characterization of six DAPEG-modified analogs of LL-37 in which (i) all five Arg residues (positions 7, 19, 23, 29, 34), (ii) all six Lys residues (positions 8, 10, 12, 15, 18, 25) or (iii) all three Ile residues (positions 13, 20, 24) were substituted with Dap derivatives bearing either a one-unit or a two-unit oxa-spacer. The aims were to (a) determine whether DAPEG substitution preserves the structural and DNA-binding features of LL-37; (b) quantify protection against proteolytic degradation and against PAD2/PAD4-mediated citrullination; (c) assess cytotoxicity and direct antibacterial activity; and (d) functionally characterize modulation of neutrophil-like cells using differentiated HL-60 cells with LPS challenge, measuring two independent degranulation markers — proteinase 3 (PR3) and myeloperoxidase (MPO) — both co-stored in azurophilic primary granules [27,28]. The concordant readout of two independent granule markers was used to discriminate genuine inhibition of degranulation from marker-specific artefacts and to strengthen the mechanistic interpretation of the inhibitory phenotype of the lead analogs.

2. Materials and Methods

2.1. Peptide Synthesis

All compounds were synthesized by Fmoc/tBu solid-phase peptide synthesis on TentaGel S-AC resin pre-loaded with serine (loading 0.24 mmol/g, 90 μm; Iris Biotech GmbH, Marktredwitz, Germany), on a 0.1 mmol scale (0.417 g resin). Backbone assembly was performed on a LibertyBlue microwave synthesiser (CEM Corporation, Matthews, NC, USA) using 0.2 M Fmoc-amino acid in DMF, 0.5 M DIC in DMF and 1.0 M Oxyma in DMF (coupling: 165 s at 90 °C). Fmoc deprotection

 doi:10.20944/preprints202606.0060.v1

used 20% piperidine/DMF (65 s at 90 °C). At positions of intended modification, Fmoc-Dap(ivDde)-OH was incorporated.

After backbone assembly, ivDde side-chain protecting groups were removed by 2% anhydrous hydrazine in DMF (6 × 15 min). Side-chain acylation with Boc/Pbf-protected oxa-acid derivatives — Boc-Pbf-guanidino-O1Pen-OH (GO1), Boc-Pbf-guanidino-O2Oc-OH (GO2), Boc-O1Pen-OH (O1) or Boc-O2Oc-OH (O2) — was performed in DMF/NMP/DCM (1:1:1, v/v/v) with trace Triton X-100, activated with DIC and Oxyma, in three sequential cycles at 2×, 1.5× and 1.0× molar excess. Cleavage and global deprotection: TFA/phenol/water/thioanisole/ethanedithiol (82.5/5/5/5/2.5, v/v/v/v/v; 4 h, room temperature). Crude products were precipitated with cold diethyl ether, redissolved in deionized water, lyophilized and purified by RP-HPLC.

2.2. Analytical Characterization

Mass: MALDI-TOF MS (Bruker Biflex III). Purity: UPLC on Shimadzu Nexera X2 LC-30AD with Phenomenex Aeris Peptide XB-C18 (150 × 2.1 mm, 1.7 µm); gradient 3–90% B over 22 min at 0.4 mL/min. Circular dichroism: 0.2 mg/mL in 50% TFE/water, pH ≈ 7. All measurements performed in triplicate (n = 3); mean values reported, with standard deviations in the Supplementary Information.

2.3. Proteolytic Stability Against Proteinase 3

Reactions: 45 µM peptide and 0.2 µM recombinant human PR3 in 10 mM Tris-HCl/0.01% ammonium acetate, pH 7.5, 37 °C. Aliquots at 0, 1, 2, 4, 6 and 24 h analyzed by LC-MS (Bruker HCT Ultra ion trap; Phenomenex Gemini-NX 5µ C18, 4.6 × 150 mm; 10–90% acetonitrile/0.1% formic acid over 50 min). Half-lives (t1/2) were derived from monoexponential decay fits performed by nonlinear least-squares regression in GraphPad Prism 10 (GraphPad Software, San Diego, CA); fit quality was assessed by R^2 and 95% confidence intervals for t1/2 are reported alongside point estimates. Pairwise comparison of analog t1/2 versus native LL-37 was performed by ordinary one-way ANOVA with Dunnett post hoc multiple comparisons test; significance threshold $p < 0.05$. n = 3 independent reactions per condition; data reported as mean ± SD.

2.4. PAD2 and PAD4 Citrullination Assay

PAD2 (3.34 µM) or PAD4 (1.35 µM) with 50 µM peptide in 0.24 M Tris-HCl/0.05 M CaCl2, pH 7.6, 37 °C. Aliquots at 0, 2, 4, 6, 8 and 24 h analyzed by LC-MS. Each Arg → Cit conversion produces +1 Da increment. Citrullination assays were performed for native LL-37 and the Arg-substituted analogs Dap(GO1)[7,19,23,29,34]LL-37 and Dap(GO2)[7,19,23,29,34]LL-37 only, since the Lys- and Ile-substituted analogs do not contain arginine residues accessible to PAD-mediated deimination. Time-course mass shifts were compared between native LL-37 and Arg-substituted analogs by two-way repeated-measures ANOVA (factors: compound, time) with Sidak correction for multiple comparisons in GraphPad Prism 10; significance threshold $p < 0.05$. n = 3 independent reactions per condition; data reported as mean ± SD.

2.5. DNA-Binding Studies

Agarose gel electrophoresis (0.8% agarose, TBE, Midori Green) with pUC19 plasmid (2688 bp) at N/P 1:1 and 5:1. PAGE (4%/8% gels, TAE) with synthetic 76-bp dsDNA. Microscale thermophoresis (Monolith NT.115, NanoTemper) with Cy5-labeled 76-bp dsDNA (100 nM) and serial peptide dilutions (200 µM starting, 16-fold dilution); three buffer systems tested (EDBS; PBS/0.05% Tween-20; PBS/0.1% Pluronic F-127); three independent replicates per condition. AFM imaging (BioScope Resolve, Bruker; ScanAsystFluid+) of peptide–pUC19 complexes (N/P = 0.2:1, 8 mM MgCl2, 5 nM pUC19, 0.875 nM peptide; Dr K. Bury, Intercollegiate Faculty of Biotechnology UG/MUG); images shown in Figure 3 are representative of three independent preparations per peptide; quantitative field-by-field analysis was not performed. Dynamic light scattering and zeta potential (Litesizer DLS 500, Anton Paar; Dr B. Szafranek, Physicochemical Measurements Laboratory); n = 3 measurements

 doi:10.20944/preprints202606.0060.v1

per sample. DLS hydrodynamic diameters across peptide–DNA complexes were compared by ordinary one-way ANOVA with Tukey multiple comparisons test in GraphPad Prism 10; significance threshold $p < 0.05$.

2.6. Antibacterial Activity

Minimum inhibitory concentration (MIC) by broth microdilution per CLSI guidelines, with reference strains *Escherichia coli* ATCC 25922, *Staphylococcus aureus* ATCC 25923 and *Pseudomonas aeruginosa* ATCC 27853. Bacterial inoculum 5×10^5 CFU/mL in cation-adjusted Mueller-Hinton broth. Compounds tested at 1, 2, 4, 8, 16, 32 and 64 μM for 18–20 h at 37 °C. MIC defined as lowest concentration with no visible growth. Each MIC plate included a sterility control (broth alone), a growth control (broth + inoculum, no peptide), and a positive antibiotic control with a reference compound at known CLSI-defined MIC range; only plates passing all three controls were retained for analysis. Each compound tested in n = 3 biological replicates with technical duplicates.

2.7. Cell Culture

HB2 (breast epithelial), CRL-1472 (bladder transitional carcinoma stage III; ATCC), HDFa (primary dermal fibroblasts) and HL-60 (promyelocytic leukemia; ATCC CCL-240) cell lines were obtained from ATCC or commercial suppliers and used within 10 passages from receipt. All lines were routinely tested for mycoplasma contamination by PCR and were mycoplasma-free throughout the study. Cells were maintained at 37 °C, 5% CO2 in their respective media (full composition details in Supplementary Information, Section S1). For neutrophil-like differentiation, HL-60 cells were cultured in RPMI-1640 + 10% FBS + 1% penicillin/streptomycin + 1.25% DMSO for five days with daily medium exchange and cell count regulation to 10×10^6 cells. Differentiation to a neutrophil-like phenotype was monitored by morphological assessment and surface marker expression (data not shown)

2.8. MTT Cytotoxicity Assay

Cells were seeded at 5×10^4 cells/well in 96-well plates 48 h prior to treatment. Compounds were applied at 1, 5, 10, 20 and 50 μM for 24 h. MTT (5 mg/mL in PBS) was added, plates were incubated 4 h at 37 °C, formazan crystals were solubilized in DMSO, and absorbance was read at 570 nm (SPECTROstar Nano, BMG LabTech). Cell viability was expressed as percentage relative to vehicle-treated controls. IC50 values, where determinable from the dose–response curve, were calculated by non-linear regression in GraphPad Prism 10. n = 3 biological replicates with three technical replicates each; one-way ANOVA with Dunnett post hoc vs untreated control; significance $p < 0.05$.

2.9. Neutrophil-Like HL-60 Degranulation Assays — Proteinase 3 and Myeloperoxidase

On day 5 of differentiation, HL-60 cells (5×10^6 cells/well, 0.1% fish gelatin-coated 6-well plates) were exposed to compounds at 5.05 μM for 1 h or 24 h at 37 °C, followed by LPS challenge (0.198 μM, 45 min). These working concentrations correspond to standardized serial dilutions from peptide and LPS stock solutions used throughout this study; the peptide concentration is within the conventional in vitro working range (1–10 μM) for LL-37 in primary neutrophil and HL-60 systems. Extracellular medium was collected. The same supernatants were used for both PR3 and MPO assays to ensure direct comparability of the two markers.

PR3 activity: measured using the internally quenched fluorescent (IQF) substrate ABZ-Tyr-Tyr-Abu-Asn-Glu-Pro-Dap(DNP)-NH2 (final concentration 4.73×10^{-5} M), in which the ortho-aminobenzoic acid (ABZ) fluorophore is FRET-quenched by the 2,4-dinitrophenyl (DNP) acceptor introduced on the Dap side chain; proteolytic cleavage of the scissile bond between the ABZ donor and DNP acceptor releases the donor fluorescence (excitation maximum λ_ex = 320 nm; emission maximum λ_em = 450 nm). To confirm that the fluorescent signal originated specifically from PR3 activity, parallel reactions were performed with the selective phosphonate-based PR3 inhibitor Bt-

 doi:10.20944/preprints202606.0060.v1

Pro-Tyr-Asp-AbuP(O-C6H4-4-Cl)2 (final concentration 4.71 × 10^{-6} M, ≈ 10-fold molar excess over substrate to ensure complete active-site occupancy). Reactions were conducted in 100 mM Tris-HCl / 500 mM NaCl, pH 7.5; fluorescence kinetics were recorded on a CLARIOstar plate reader (BMG LabTech) in continuous kinetic mode at 37 °C. Initial reaction rates were calculated as the slope of the linear portion of the fluorescence-versus-time curve (typically the first 5–10 min) using linear regression in MARS Data Analysis software (BMG LabTech). PR3-specific activity was defined as the difference between the slope in the absence of inhibitor and the slope in the parallel inhibitor-containing reaction (slope_uninhibited − slope_inhibited), expressed in arbitrary fluorescence units per second (a.u./s).

MPO activity: measured fluorometrically in the same supernatants using the Myeloperoxidase (MPO) Peroxidation Activity Assay Kit (Fluorometric) (Abcam, ab111749), per the manufacturer's protocol. n = 3 biological replicates per condition with technical duplicates; two-way ANOVA with Sidak correction for multiple comparisons. Data shown as mean ± SD.

2.10. Statistical Analysis

All statistical analyses were performed in GraphPad Prism 10.0 (GraphPad Software, San Diego, CA, USA). Data are presented as mean ± standard deviation (SD) unless otherwise stated. Normality of distribution was assessed by the Shapiro–Wilk test prior to parametric testing. The following tests were applied: (i) proteolytic half-lives versus native LL-37 — ordinary one-way ANOVA with Dunnett post hoc multiple comparisons test (Section 2.3); (ii) PAD2/PAD4 time-course mass shifts — two-way repeated-measures ANOVA (factors: compound, time) with Sidak correction for multiple comparisons (Section 2.4); (iii) DLS hydrodynamic diameters — ordinary one-way ANOVA with Tukey post hoc multiple comparisons test (Section 2.5); (iv) MTT viability vs untreated control — ordinary one-way ANOVA with Dunnett post hoc (Section 2.8); (v) PR3 and MPO degranulation responses — two-way ANOVA (factors: compound, LPS) with Sidak correction (Section 2.9). For all tests, the threshold of statistical significance was set at $p < 0.05$; in figures, statistical significance is indicated as * $p < 0.05$, ** $p < 0.01$, *** $p < 0.001$. Sample size (n) refers to independent biological replicates throughout, with technical replicates per biological replicate indicated where applicable in each Methods subsection.

3. Results

3.1. Synthesis and Physicochemical Characterization

All six DAPEG analogs and native LL-37 were obtained by Fmoc/tBu SPPS. MALDI-TOF mass spectrometry confirmed identity within 3.5 Da of theoretical values (Table 1). UPLC retention times ranged from 8.06 to 8.52 min. Purification yields after RP-HPLC were 38–45% of theoretical, consistent with typical performance for 37-residue peptides containing multiple non-canonical residues. A pilot synthesis of a fourth, phenylalanine-substituted series was attempted but did not yield products matching theoretical masses and is the subject of ongoing optimization (details in Supplementary Information).

Table 1. Molecular masses (measured and theoretical, MALDI-TOF MS) and UPLC retention times of LL-37 and the six DAPEG analogs. Δ: difference between measured and theoretical mass.

No.	Compound	Measured MW [Da]	Theoretical MW [Da]	Δ [Da]	tR [min]
1a	Dap(GO1)[7,19,23,29,34]LL-37	4860.38	4858.60	1.78	8.47
1b	Dap(GO2)[7,19,23,29,34]LL-37	5079.98	5078.86	1.12	8.06
2a	Dap(O1)[8,10,12,15,18,25]LL-37	4850.19	4847.41	2.78	8.52
2b	Dap(O2)[8,10,12,15,18,25]LL-37	5115.05	5111.72	3.33	8.43

 doi:10.20944/preprints202606.0060.v1

No.	Compound	Measured MW [Da]	Theoretical MW [Da]	Δ [Da]	tR [min]
3a	Dap(MO1)[13,20,24]LL-37	4763.05	4760.41	2.64	8.26
3b	Dap(MO2)[13,20,24]LL-37	4894.99	4892.57	2.42	8.44
LL-37	LLGDFFRKSKEKIGKEFKRIVQ RIKDFLRNLVPRTES	4491.34	4492.14	0.80	—

3.2. Secondary Structure

Circular dichroism spectra in 50% TFE/water at pH ≈ 7 (Figure 1) revealed three distinct profiles. The arginine-substituted Dap(GO1)[7,19,23,29,34]LL-37 and Dap(GO2)[7,19,23,29,34]LL-37 analogs yielded spectra closely matching native LL-37 with characteristic minima near 208 and 222 nm and comparable signal intensity, confirming that the guanidinium-bearing oxa-acid side chain preserves the helix-stabilizing contribution of arginine. The isoleucine-substituted Dap(MO1)[13,20,24]LL-37 and Dap(MO2)[13,20,24]LL-37 analogs showed slightly reduced minimum intensities, consistent with partial helix destabilization. The lysine-substituted Dap(O1)[8,10,12,15,18,25]LL-37 and Dap(O2)[8,10,12,15,18,25]LL-37 analogs retained the helical fingerprint but with markedly reduced signal intensity, indicating markedly lower helical content — the expected consequence of replacing six cationic Lys residues with neutral oxa-acid side chains and reducing the driving force for helix induction at the membrane interface [5,6,12].

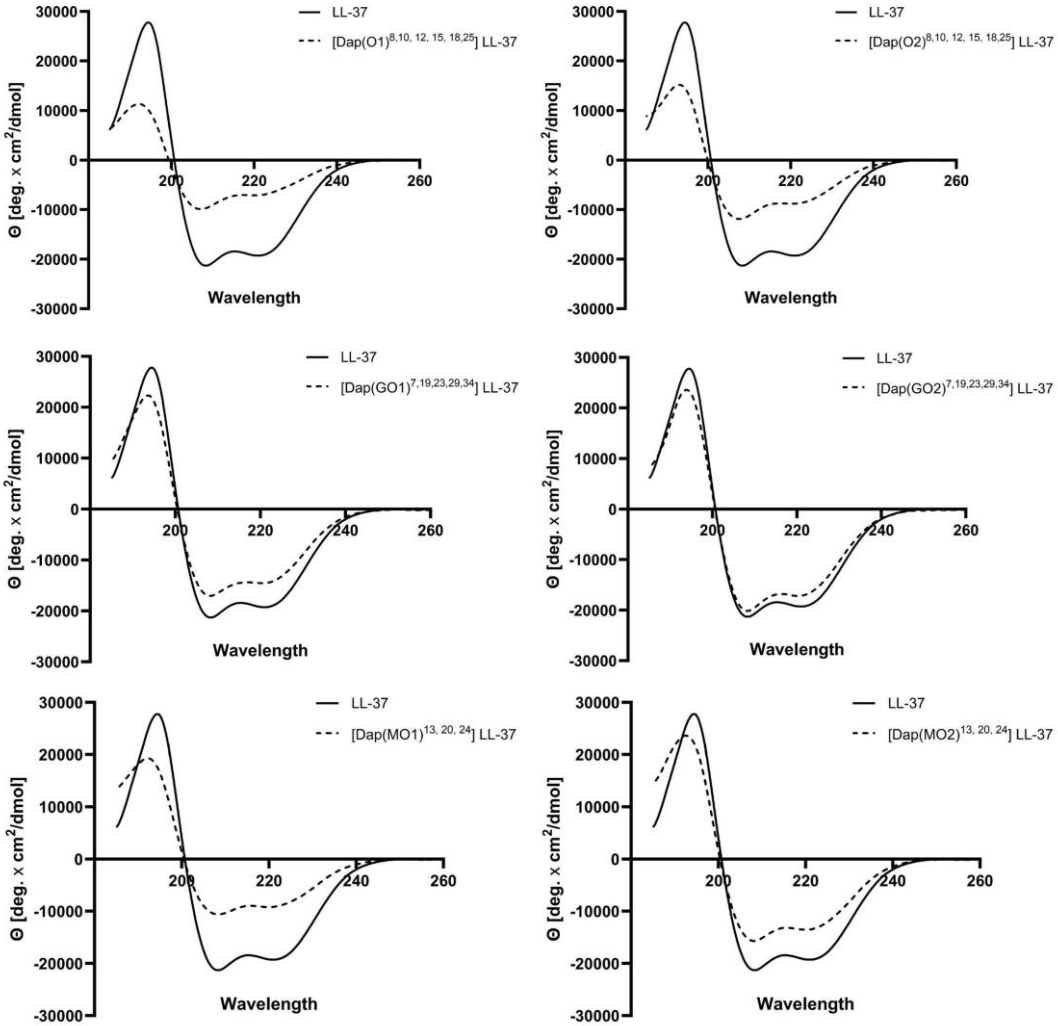

 doi:10.20944/preprints202606.0060.v1

Figure 1. Circular dichroism spectra of LL-37 and the six DAPEG analogs in 50% TFE/water, pH ≈ 7. Each panel overlays the analog (dashed) on native LL-37 (solid). Top row: Dap(O1)[8,10,12,15,18,25]LL-37 (left) and Dap(O2)[8,10,12,15,18,25]LL-37 (right) — markedly reduced helical content. Middle row: Dap(GO1)[7,19,23,29,34]LL-37 (left) and Dap(GO2)[7,19,23,29,34]LL-37 (right) — helical fingerprint preserved. Bottom row: Dap(MO1)[13,20,24]LL-37 (left) and Dap(MO2)[13,20,24]LL-37 (right) — intermediate, partial helix destabilization. Y-axis: Θ [deg × cm²/dmol]; X-axis: wavelength [nm].

3.3. Proteolytic Stability Against Proteinase 3

Resistance to PR3-mediated degradation was strongly dependent on both modification site and oxa-spacer length (Table 2, Figure 2). Native LL-37 was rapidly degraded (t1/2 = 130.2 min), primarily through cleavage at the Val21–Gln22 bond, generating fragments of 2537.24 Da and 2183.92 Da. The Dap(GO1)[7,19,23,29,34]LL-37 analog exhibited the strongest stabilization — t1/2 = 740.4 min, a 5.7-fold improvement — with slow, nearly linear degradation over 24 h. By contrast, the longer-spacer Dap(GO2)[7,19,23,29,34]LL-37 analog (t1/2 = 120.4 min) was marginally less stable than native LL-37, and only a single hydrolysis fragment was detectable. The lysine-substituted Dap(O1)[8,10,12,15,18,25]LL-37 (t1/2 = 242.31 min) and Dap(O2)[8,10,12,15,18,25]LL-37 (t1/2 = 306.21 min) showed intermediate 1.9- and 2.4-fold improvements. The isoleucine-substituted Dap(MO1)[13,20,24]LL-37 (t1/2 = 16.47 min) and Dap(MO2)[13,20,24]LL-37 (t1/2 = 44.41 min) displayed reduced stability relative to native LL-37, indicating that DAPEG substitution at Ile positions actually destabilizes the central helix region against PR3 attack.

Table 2. PR3-mediated proteolysis kinetics. Half-lives (t1/2) and major fragment masses; fold-change relative to native LL-37. Mean of n = 3 independent enzymatic reactions per condition.

Compound	t1/2 [min]	Fragment 1 MW [Da]	Fragment 2 MW [Da]	vs LL-37
LL-37	130.2	2537.24 (Val21↓)	2183.92 (Ile13/Leu28)	1.0×
Dap(GO1)[7,19,23,29,34]LL-37	740.4	2852.54	2393.32	5.7×
Dap(GO2)[7,19,23,29,34]LL-37	120.4	3026.84	—	0.9×
Dap(O1)[8,10,12,15,18,25]LL-37	242.31	2832.24	2360.38	1.9×
Dap(O2)[8,10,12,15,18,25]LL-37	306.21	3052.59	2492.53	2.4×
Dap(MO1)[13,20,24]LL-37	16.47	2743.40	2389.16	0.13×
Dap(MO2)[13,20,24]LL-37	44.41	2831.50	2477.58	0.34×

 doi:10.20944/preprints202606.0060.v1

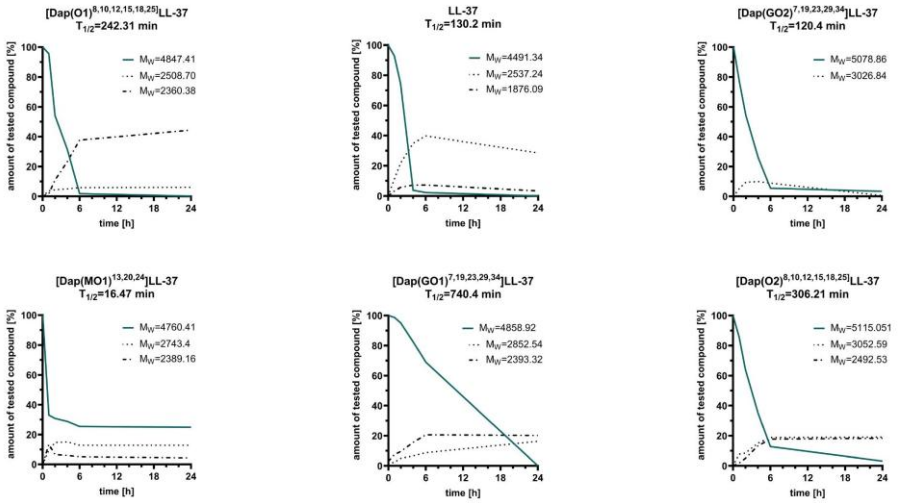

Figure 2. PR3 proteolysis kinetics over 24 h, monitored by LC-MS. Each panel shows intact peptide (solid line) and hydrolysis fragments (dotted/dashed); t1/2 values shown above each panel.

3.4. Resistance to PAD2- and PAD4-Mediated Citrullination

Citrullination of arginine residues was quantified by LC-MS as +1 Da mass shifts (Table 3). Native LL-37 underwent a +4 Da mass increase by 6 h with both PAD2 and PAD4, consistent with citrullination of approximately four of its five arginines. The Dap(GO1)[7,19,23,29,34]LL-37 analog showed delayed citrullination, with mass shift not detectable until 4–6 h. The Dap(GO2)[7,19,23,29,34]LL-37 analog conferred the highest resistance: the first +1 Da shift appeared only at 6 h, and the total shift at 24 h corresponded to citrullination of just a single side chain. The longer two-unit oxa-spacer thus provides superior steric shielding of the guanidinium group from the PAD active site, despite the same spacer giving inferior PR3 protection (Section 3.3). This position- and target-specific dependence on spacer length is mechanistically informative and discussed in Section 4.3.

Table 3. Molecular mass evolution during incubation with PAD2 or PAD4. Each +1 Da increment corresponds to one Arg → Cit conversion. Selected timepoints from the full kinetic series described in Section 2.4 are shown to highlight the differential progression of citrullination. Masses in Da; mean of n = 3 independent reactions.

Enzyme / Compound	t = 0 h	t = 2 h	t = 6 h	t = 8 h	t = 24 h
PAD2 / LL-37	4491.3	4494.3	4495.3	4495.3	4495.3
PAD2 / Dap(GO1)[7,19,23,29,34]LL-37	4858.60	4858.60	4859.60	4860.60	4860.60
PAD2 / Dap(GO2)[7,19,23,29,34]LL-37	5078.60	5078.60	5079.60	5079.60	5079.60
PAD4 / LL-37	4491.3	4494.3	4495.3	4495.3	4495.3
PAD4 / Dap(GO1)[7,19,23,29,34]LL-37	4858.60	4858.60	4859.60	4860.60	4860.60
PAD4 / Dap(GO2)[7,19,23,29,34]LL-37	5078.60	5078.60	5079.60	5079.60	5079.60

3.5. DNA-Binding Capacity

 doi:10.20944/preprints202606.0060.v1

All DAPEG analogs retained DNA-binding capacity by qualitative agarose gel electrophoresis and AFM imaging. AFM at N/P = 0.2:1 (Figure 3) showed condensed peptide–pUC19 complexes morphologically similar to those formed by native LL-37, with subtle geometric differences between analogs. Microscale thermophoresis was attempted but did not yield reliable K*d* values: three independent fits for native LL-37 gave widely divergent values (33.8, 96.9 and 62 µM), spanning a 2.9-fold range. This precludes quantitative ranking of analog affinities; complementary methods (ITC, BLI, fluorescence anisotropy) are required.

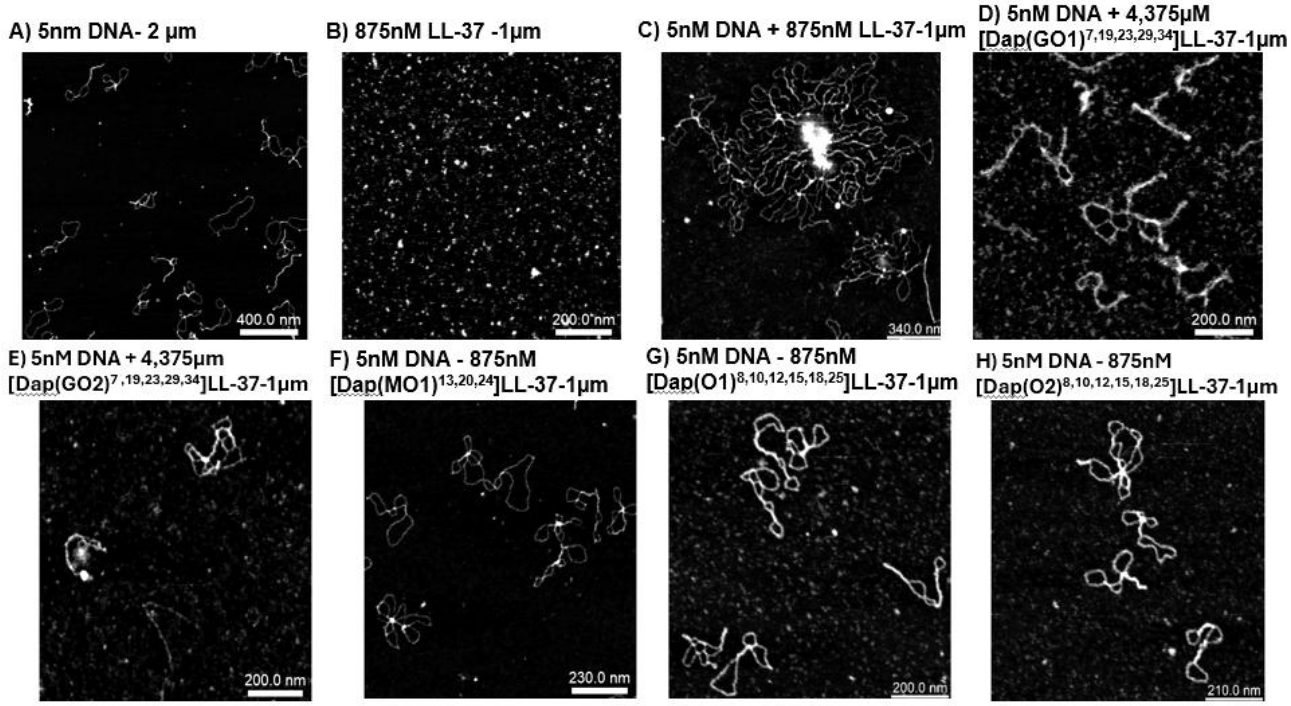

Figure 3. AFM imaging of peptide–pUC19 complexes (N/P = 0.2:1, 8 mM MgCl2, 5 nM pUC19). A) pUC19 alone (scale 400 nm); B) LL-37 alone (200 nm); C) LL-37 + pUC19 (340 nm); D) Dap(GO1)[7,19,23,29,34]LL-37 + pUC19 (200 nm); E) Dap(GO2)[7,19,23,29,34]LL-37 + pUC19 (200 nm); F) Dap(MO1)[13,20,24]LL-37 + pUC19 (230 nm); G) Dap(O1)[8,10,12,15,18,25]LL-37 + pUC19 (200 nm); H) Dap(O2)[8,10,12,15,18,25]LL-37 + pUC19 (210 nm). Imaging by Dr K. Bury (IFB UG/MUG).

Dynamic light scattering revealed a quantitative gradient not apparent in qualitative assays (Figure 4). Complexes of native LL-37, Dap(GO1)[7,19,23,29,34]LL-37 and Dap(GO2)[7,19,23,29,34]LL-37 with dsDNA condensed to compact particles (≈ 50–100 nm), smaller than free dsDNA (≈ 580 nm). By contrast, Dap(O1)[8,10,12,15,18,25]LL-37 and Dap(O2)[8,10,12,15,18,25]LL-37 complexes formed larger particles (≈ 330–370 nm), suggesting less efficient compaction or higher-order aggregation — mechanistically coherent with their reduced cationic character and helical content.

 doi:10.20944/preprints202606.0060.v1

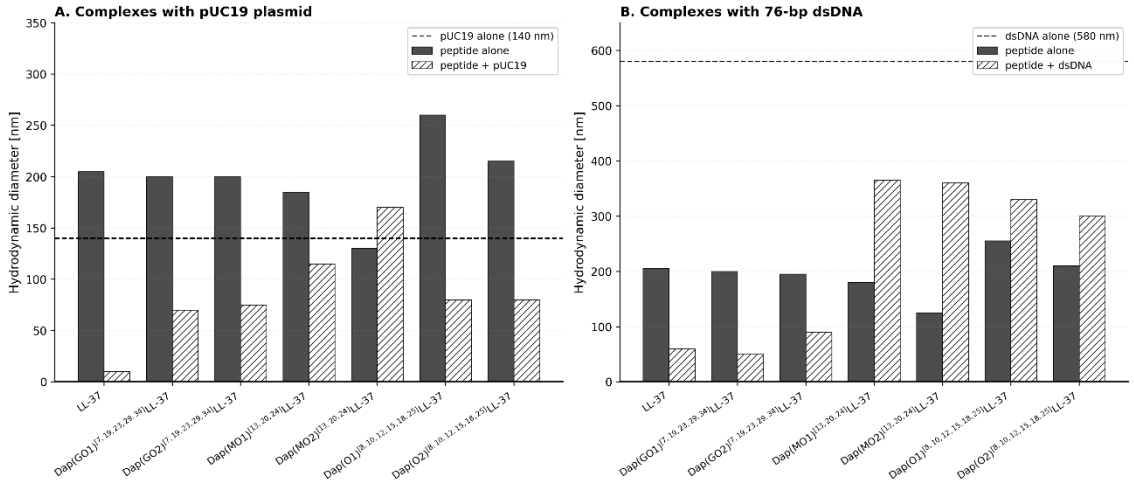

Figure 4. DLS particle-size measurements of peptidomimetics and their complexes. Left panel: complexes with pUC19 plasmid; right panel: complexes with 76-bp dsDNA. Y-axis: hydrodynamic diameter (nm). Mean of n = 3 measurements per condition.

3.6. Antibacterial Activity

Minimum inhibitory concentration assays against three reference bacterial strains revealed a striking and uniform result (Table 4): only native LL-37 retained antibacterial activity, while all six DAPEG analogs were inactive at concentrations up to 64 μM against *E. coli* ATCC 25922, *S. aureus* ATCC 25923 and *P. aeruginosa* ATCC 27853. The complete loss of direct antibacterial activity across all modification classes — including the helix-preserving Arg-substituted analogs — indicates that the DAPEG modifications, despite leaving secondary structure largely intact, disrupt the productive membrane-disruption capacity of the LL-37 scaffold. This finding fundamentally reframes the DAPEG strategy: the modifications do not improve LL-37 as an antibacterial peptide but reprofile it toward immunomodulatory function (Section 4.2).

Table 4. Antibacterial activity (minimum inhibitory concentration, MIC) against three reference strains. Numerical MIC values for native LL-37 (in μM) are given in parentheses; literature ranges are 2–8 μM for E. coli, 4–16 μM for S. aureus and 2–8 μM for P. aeruginosa under standard CLSI conditions. "Inactive" indicates no growth inhibition at concentrations up to 64 μM. n = 3 biological replicates with technical duplicates per condition.

Compound	E. coli	S. aureus	P. aeruginosa	MIC range tested
LL-37	active	active	active	1–64 μM
Dap(GO1)[7,19,23,29,34]LL-37	inactive	inactive	inactive	1–64 μM
Dap(GO2)[7,19,23,29,34]LL-37	inactive	inactive	inactive	1–64 μM
Dap(O1)[8,10,12,15,18,25]LL-37	inactive	inactive	inactive	1–64 μM
Dap(O2)[8,10,12,15,18,25]LL-37	inactive	inactive	inactive	1–64 μM
Dap(MO1)[13,20,24]LL-37	inactive	inactive	inactive	1–64 μM
Dap(MO2)[13,20,24]LL-37	inactive	inactive	inactive	1–64 μM

3.7. Cytotoxicity

MTT assays at 24 h across five cell systems showed no cytotoxicity at 1–10 μM for any compound (Table 5). The lysine-substituted Dap(O1)[8,10,12,15,18,25]LL-37 and Dap(O2)[8,10,12,15,18,25]LL-37 and

 doi:10.20944/preprints202606.0060.v1

isoleucine-substituted Dap(MO1)[13,20,24]LL-37 and Dap(MO2)[13,20,24]LL-37 analogs were fully non-toxic up to 50 μM against HDFa fibroblasts. CRL-1472 bladder carcinoma cells were selectively sensitive at 50 μM to all compounds. Differentiated HL-60 cells showed increased viability with all compounds, consistent with the pro-survival effect of LL-37 on neutrophils through PI3K/Akt signaling [8]. The combination of complete non-cytotoxicity in normal cells with absence of antibacterial activity (Section 3.6) defines an unusual but pharmacologically interesting profile: high biocompatibility without direct microbicidal action.

Table 5. MTT cytotoxicity at 24 h. NT — non-toxic (cell viability not significantly different from untreated control, $p \geq 0.05$); T — toxic at indicated concentration (cell viability significantly reduced, $p < 0.05$); ↑ viability — increased relative to untreated control. Numerical viability values (mean ± SD) and IC50 estimates where determinable are provided in the Supplementary Information (Table S2). n = 3 biological replicates; one-way ANOVA with Dunnett post hoc.

Compound	HDFa	HB2	CRL-1472	HL-60	HL-60 (diff.)
LL-37	NT 1–10 μM	NT 1–20 μM	NT 1–10 μM; T at 50 μM	NT	NT; ↑ viability
Dap(GO1)[7,19,23,29,34]LL-37	NT 1–10 μM	NT 1–20 μM	NT 1–10 μM; T at 50 μM	NT	NT; ↑ viability
Dap(GO2)[7,19,23,29,34]LL-37	NT 1–10 μM	NT 1–20 μM	NT 1–10 μM; T at 50 μM	NT	NT; ↑ viability
Dap(O1)[8,10,12,15,18,25]LL-37	NT 1–50 μM	NT 1–20 μM	NT 1–20 μM; T at 50 μM	NT	NT
Dap(O2)[8,10,12,15,18,25]LL-37	NT 1–50 μM	NT 1–20 μM	NT 1–20 μM; T at 50 μM	NT	NT
Dap(MO1)[13,20,24]LL-37	NT 1–50 μM	NT 1–20 μM	NT 1–20 μM; T at 50 μM	NT	NT; moderate suppress.
Dap(MO2)[13,20,24]LL-37	NT 1–50 μM	NT 1–20 μM	NT 1–20 μM; T at 50 μM	NT	NT; moderate suppress.

3.8. Modulation of Neutrophil-Like HL-60 Degranulation: Concordant PR3 and MPO Readouts

The most pharmacologically novel findings of this study were obtained by measuring two independent markers of azurophilic granule release — proteinase 3 (PR3) and myeloperoxidase (MPO) — from the same supernatants of differentiated HL-60 cells exposed to peptides at 5.05 μM, with or without subsequent LPS challenge. The two-marker design discriminates between genuine inhibition of degranulation and assay-specific artefacts: concordant suppression of both PR3 and MPO indicates a true effect on granule release, while marker-specific responses would imply alternative mechanisms (e.g., direct enzyme inhibition or selective signaling).

Arginine-substituted analogs (Figures 5C, 6C). Dap(GO1)[7,19,23,29,34]LL-37 and Dap(GO2)[7,19,23,29,34]LL-37 produced a biphasic phenotype distinct from native LL-37. At 1 h, both compounds activated PR3 and MPO release comparably to LL-37 + LPS (no significant difference in the LPS-stimulated condition; Sidak post-hoc $p > 0.05$). By 24 h, however, MPO secretion in the analog

 doi:10.20944/preprints202606.0060.v1

+ LPS conditions was significantly reduced relative to LL-37 + LPS: Dap(GO1)[7,19,23,29,34]LL-37 + LPS reduced MPO to 21.67 ± 1.64 a.u. versus 31.78 ± 0.95 a.u. for LL-37 + LPS ($p = 0.003$ by Sidak post-hoc), and Dap(GO2)[7,19,23,29,34]LL-37 + LPS to 23.43 ± 2.70 a.u. ($p = 0.028$). The two-way ANOVA confirmed a significant compound × time interaction ($F(7,32) = 25.00$, $p < 0.0001$), indicating that the modulatory effect of arginine substitution is temporally dynamic — an initial activation phase followed by attenuation that exceeds the natural decay seen for LL-37 itself. The two markers (PR3 and MPO) were highly concordant across both time points.

Lysine-substituted analogs (Figures 5A, 6A) — primary anti-inflammatory phenotype. Dap(O1)[8,10,12,15,18,25]LL-37 and Dap(O2)[8,10,12,15,18,25]LL-37 did not induce baseline PR3 or MPO release. On LPS challenge these analogs **markedly reduced both PR3 and MPO secretion relative to LL-37 + LPS**: at 1 h, MPO activity was 1.06 ± 0.04 a.u. for Dap(O1)[8,10,12,15,18,25]LL-37 + LPS and 1.14 ± 0.03 a.u. for Dap(O2)[8,10,12,15,18,25]LL-37 + LPS, compared with 38.86 ± 5.09 a.u. for LL-37 + LPS (both $p < 0.001$ by Sidak post-hoc; corresponding to a ~37-fold and ~34-fold reduction, respectively). The effect persisted at 24 h: Dap(O1) + LPS = 1.31 ± 0.04 a.u. and Dap(O2) + LPS = 0.22 ± 0.02 a.u. versus 30.86 ± 0.67 a.u. for LL-37 + LPS (both $p < 0.001$), the latter representing an extraordinary ~140-fold reduction. Two-way ANOVA confirmed extremely strong main effect of compound and significant compound × time interaction (compound $F(7,32) = 482.6$, $p < 0.0001$; interaction $F(7,32) = 31.7$, $p < 0.0001$). The suppressive effect was concordant across both markers and persisted at 24 h. This represents the strongest immunosuppressive profile observed in this study. The concordance between two mechanistically independent markers stored in the same granule compartment strengthens the conclusion that this is a genuine inhibition of degranulation rather than an assay artefact.

Isoleucine-substituted analogs (Figures 5B, 6B) — partial suppression. Dap(MO1)[13,20,24]LL-37 and Dap(MO2)[13,20,24]LL-37 showed reduced baseline MPO release and significantly suppressed LPS-induced MPO secretion at both time points: at 1 h, Dap(MO1)[13,20,24]LL-37 + LPS = 20.05 ± 1.86 a.u. ($p < 0.05$ vs LL-37 + LPS at 38.86 ± 5.09 a.u.) and Dap(MO2)[13,20,24]LL-37 + LPS = 11.50 ± 1.27 a.u. ($p < 0.01$); at 24 h, Dap(MO1) + LPS = 17.81 ± 1.02 a.u. and Dap(MO2) + LPS = 8.36 ± 0.82 a.u., both $p < 0.001$ versus LL-37 + LPS (30.86 ± 0.67 a.u.). Two-way ANOVA: significant main effect of compound ($F(7,32) = 119.9$, $p < 0.0001$) and significant compound × time interaction ($F(7,32) = 20.8$, $p < 0.0001$). The intermediate phenotype is again concordant between the two readouts, confirming an authentic but more modest modulatory effect than that seen for the lysine-substituted analogs. A compact summary of all PR3 and MPO data is given in Table 6.

 doi:10.20944/preprints202606.0060.v1

A Lys-substituted: Dap(O1)/Dap(O2)[8, 10, 12, 15, 18, 25]LL-37

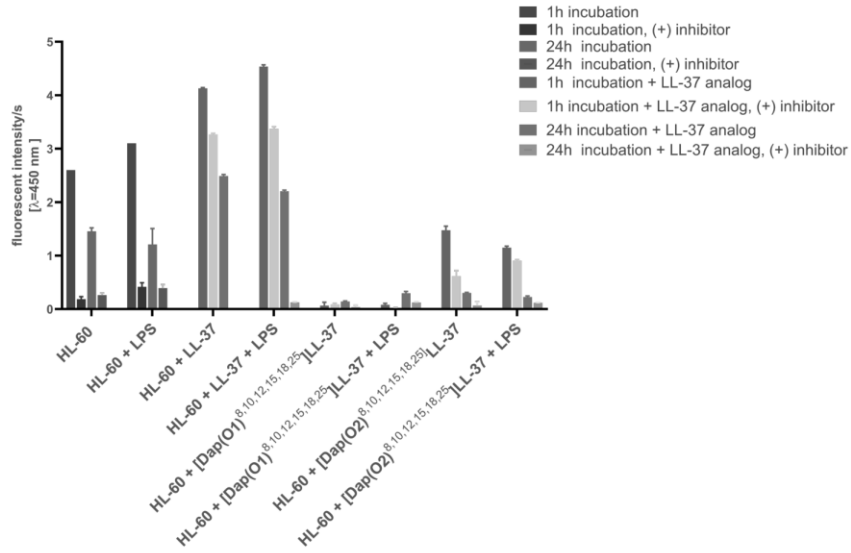

B Ile-substituted: Dap(MO1)/Dap(MO2)[13, 20, 24]LL-37

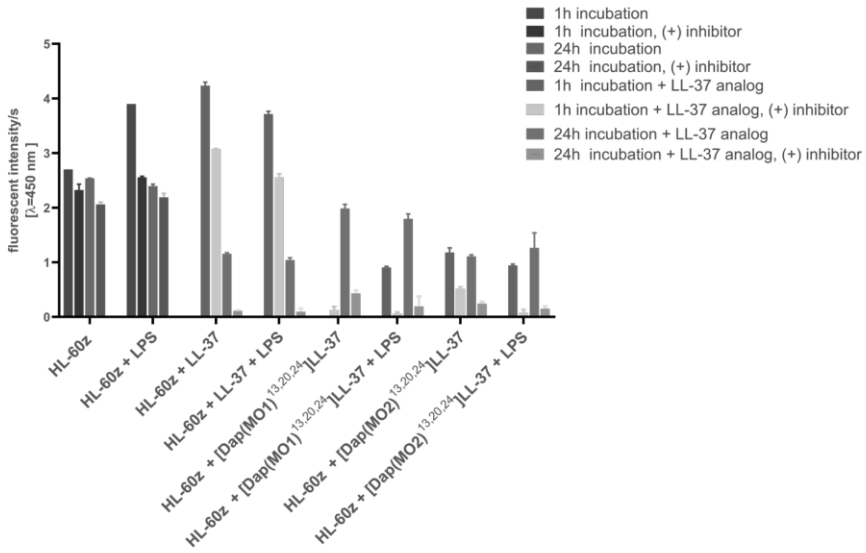

C Arg-substituted: Dap(GO1)/Dap(GO2)[7, 19, 23, 29, 34]LL-37

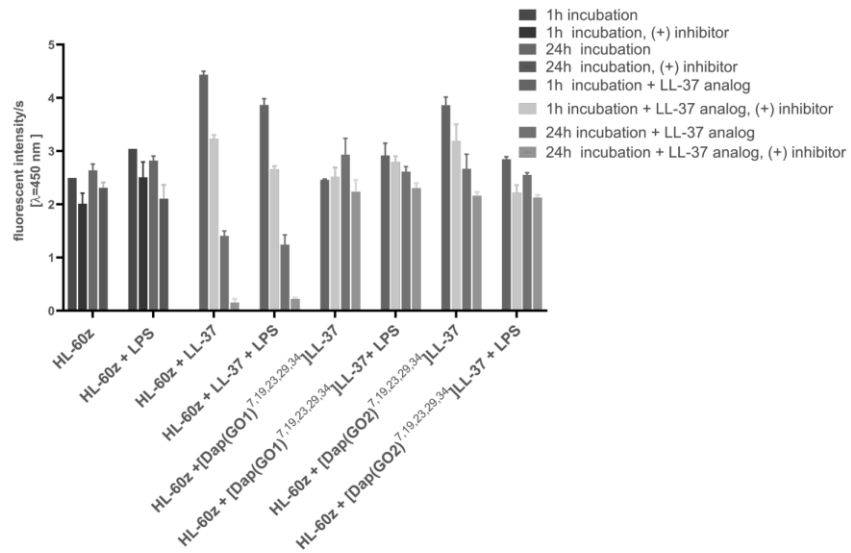

 doi:10.20944/preprints202606.0060.v1

Figure 5. Proteinase 3 secretion from differentiated HL-60 cells exposed to compounds (5.05 μM) for 1 h or 24 h, with or without LPS (0.198 μM, 45 min) and with or without selective PR3 inhibitor. A) Dap(O1)[8,10,12,15,18,25]LL-37 and Dap(O2)[8,10,12,15,18,25]LL-37; B) Dap(MO1)[13,20,24]LL-37 and Dap(MO2)[13,20,24]LL-37; C) Dap(GO1)[7,19,23,29,34]LL-37 and Dap(GO2)[7,19,23,29,34]LL-37. Y-axis: fluorescence intensity at λ = 450 nm. Mean ± SD, n = 3. Note: in-figure X-axis labels reproduce the original instrument export and use the equivalent notation [Dap(X)]^{positions}LL-37; the canonical manuscript notation Dap(X)^{[positions]}LL-37 (with positions in square brackets in superscript) is used throughout the body text and panel titles.

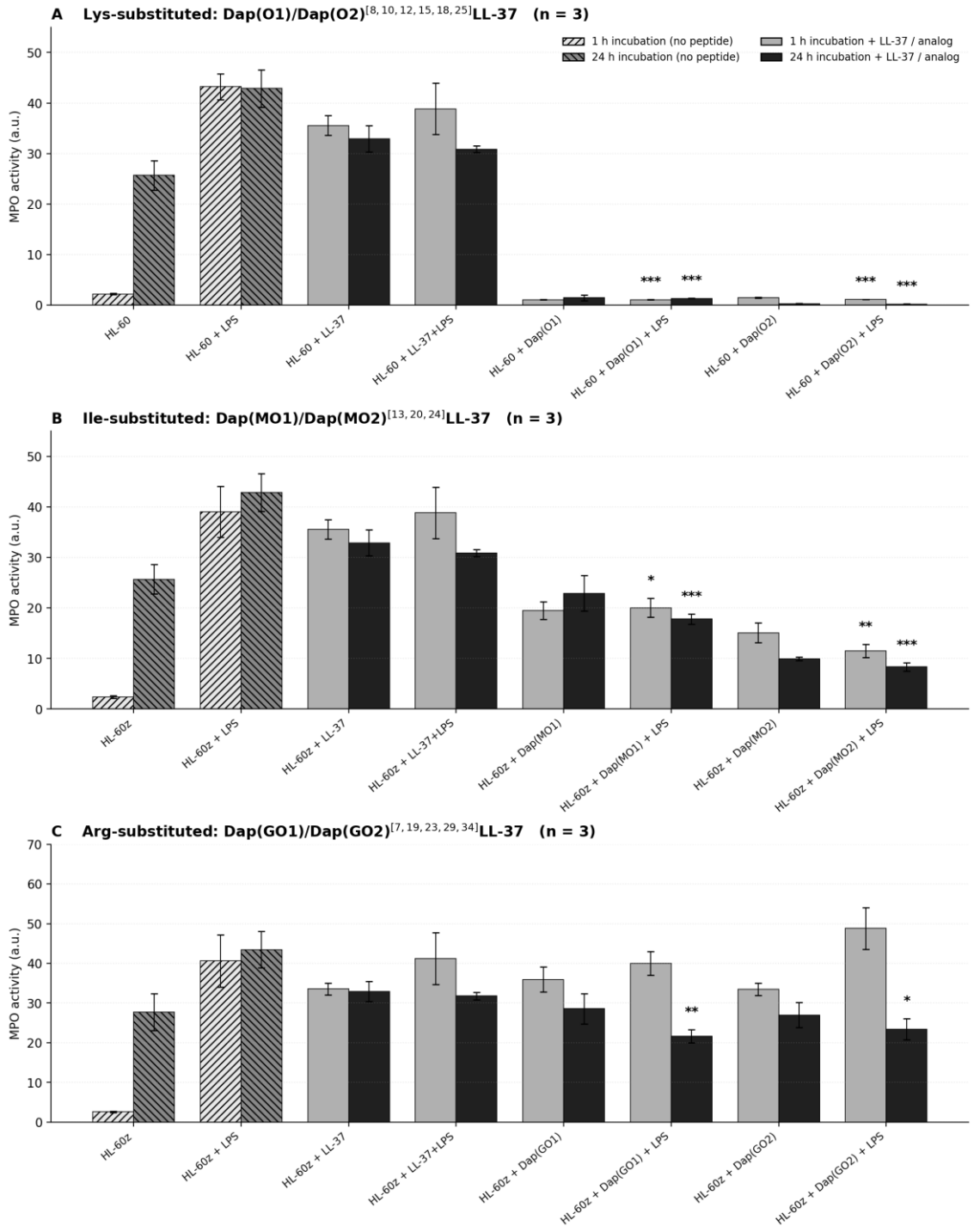

Figure 6. Myeloperoxidase activity in the same supernatants as Figure 5. A) Dap(O1)[8,10,12,15,18,25]LL-37 and Dap(O2)[8,10,12,15,18,25]LL-37; B) Dap(MO1)[13,20,24]LL-37 and Dap(MO2)[13,20,24]LL-37; C) Dap(GO1)[7,19,23,29,34]LL-37 and Dap(GO2)[7,19,23,29,34]LL-37. Concordant pattern with PR3 across all three panel families confirms that the

 doi:10.20944/preprints202606.0060.v1

suppression seen for lysine-substituted analogs is a genuine inhibition of degranulation rather than a marker-specific artefact. Data shown as mean ± SD; n = 3 biological replicates for all three panels. Statistical comparisons by two-way ANOVA (compound × time) with Sidak post-hoc test versus LL-37 + LPS at each time point: * $p < 0.05$; ** $p < 0.01$; *** $p < 0.001$. Y-axis scales differ between panels owing to assay calibration ranges; relative inter-condition relationships within each panel are the basis for biological interpretation.

Table 6. Summary of HL-60 modulation across PR3 and MPO degranulation markers, in the presence or absence of LPS. Concordant patterns between the two markers strengthen the conclusion of genuine degranulation modulation rather than enzyme-specific effects. For Arg-substituted analogs the response is biphasic — activating at 1 h, attenuated at 24 h. Statistical significance shown for MPO + LPS, where n = 3 biological replicates allowed two-way ANOVA with Sidak post-hoc versus LL-37 + LPS: * $p < 0.05$; ** $p < 0.01$; *** $p < 0.001$.

Compound	PR3 — alone	PR3 + LPS	MPO — alone	MPO + LPS
LL-37	activates	activates synergistically	activates	activates synergistically
Dap(GO1)[7,19,23,29,34]LL-37	activates	activ. 1h / reduced 24h	activates	activ. 1h / reduced 24h **
Dap(GO2)[7,19,23,29,34]LL-37	activates	activ. 1h / reduced 24h	activates	activ. 1h / reduced 24h *
Dap(O1)[8,10,12,15,18,25]LL-37	no activation	suppressed vs LL-37+LPS	no activation	suppressed vs LL-37+LPS ***
Dap(O2)[8,10,12,15,18,25]LL-37	no activation	suppressed vs LL-37+LPS	no activation	suppressed vs LL-37+LPS ***
Dap(MO1)[13,20,24]LL-37	mild activation	partial suppression	mild activation	partial suppression ***
Dap(MO2)[13,20,24]LL-37	mild activation	partial suppression	mild activation	partial suppression ***

3.9. Validation of Assay Specificity Using the PR3-Selective Inhibitor

To confirm that the fluorescent signal in the PR3 assay reflects bona fide PR3 active-site catalysis rather than non-specific proteolysis or assay artifacts, parallel reactions were performed with addition of the selective phosphonate-based PR3 inhibitor Bt-Pro-Tyr-Asp-AbuP(O-C6H4-4-Cl)2 (4.71×10^{-6} M, ≈ 10-fold molar excess over substrate). As shown in Figure 5 (light-coloured bars marked "(+) inhibitor" in each panel), addition of the inhibitor abolished the PR3-derived fluorescent signal across all conditions — baseline HL-60, LPS-stimulated HL-60, and HL-60 exposed to LL-37 or to the Dap(GO1)[7,19,23,29,34]LL-37 / Dap(GO2)[7,19,23,29,34]LL-37 analogs. Notably, the inhibitor did not abolish the MPO signal measured in parallel from the same supernatants (Figure 6C), confirming that the two-marker concordance described in Section 3.8 reflects two mechanistically independent enzymatic readouts and not cross-reactivity of the detection systems. The residual signal in the (+) inhibitor conditions (≤ 10% of uninhibited signal in most groups) provides an empirical floor for assay background and supports the conclusion that the suppression seen for the lysine-substituted Dap(O1)[8,10,12,15,18,25]LL-37 and Dap(O2)[8,10,12,15,18,25]LL-37 (Figure 5A) is a genuine reduction in PR3 release rather than a methodological artifact.

4. Discussion

4.1. DAPEG as a Modular Platform for Cathelicidin Engineering

This study demonstrates that the DAPEG framework provides a versatile platform for engineering analogs of LL-37 with tunable enzymatic stability, biocompatibility and

 doi:10.20944/preprints202606.0060.v1

immunomodulatory function. All six analogs were obtained in moderate but reproducible yields by standard Fmoc SPPS. The same Dap scaffold across all analogs, with functionality varied only by selection of oxa-acid side chain, permits combinatorial exploration of charge, hydrophobicity and helicity through orthogonal substitution at distinct residue classes — a modularity not easily achieved with stapling [16], N-methylation [17] or PEGylation [13] strategies.

4.2. Reprofiling: Loss of Antimicrobial Activity and Its Implications

The complete loss of antibacterial activity across all six DAPEG analogs against tested reference strains is the most consequential structural finding. The loss is uniform across modification classes, suggesting that the cumulative effect of multiple DAPEG insertions — even where structural parameters such as helicity are largely preserved (for the Arg-substituted analogs) — perturbs the productive lipid-bilayer-disruption interface of LL-37. The amphipathic helix functions through close geometric matching of cationic and hydrophobic faces with anionic phospholipid headgroups and acyl chains [3,4,15]; introduction of even moderately bulky oxa-acid spacers, regardless of charge type, disturbs this geometry sufficiently to abolish microbicidal function.

This requires explicit reframing of the strategy. The analogs are not improved antibacterial peptides; they are derivatives of LL-37 in which antibacterial function has been traded for enhanced enzymatic stability and — in the case of Dap(O1)$^{[8,10,12,15,18,25]}$LL-37 and Dap(O2)$^{[8,10,12,15,18,25]}$LL-37 — a substantial anti-inflammatory phenotype. This trade-off is consistent with the established SAR principle that minor perturbations of LL-37 amphipathicity disproportionately affect membrane activity [5,6,12], and with the broader observation that cationic AMP scaffolds tolerate broader perturbation for receptor-mediated immunomodulation than for direct antibacterial function [13,25,31]. The pharmacological implication is significant: clinical indications exist where LL-37 immunomodulatory activity is therapeutically desirable without the autoimmune complications of citrullinated LL-37–DNA complexes [10,11,30], and where direct antibacterial activity is neither required nor desired — chronic non-infectious inflammatory disease, immune-mediated wound healing, sterile inflammation. The DAPEG-modified analogs described here may be more appropriate for such indications than native LL-37 or stapled/SAAP-148-type variants designed to maximize antimicrobial potency [14,16].

4.3. Position- and Target-Specific Proteolytic and PAD Stabilization

The 5.7-fold protease-stabilization achieved by Dap(GO1)$^{[7,19,23,29,34]}$LL-37 is comparable to gains reported for hydrocarbon-stapled [16] and N-methylated [17] LL-37 analogs, but is obtained without introducing additional hydrophobicity that would elevate hemolytic risk. The non-linear dependence on oxa-spacer length — GO1 > GO2 for PR3 stability; GO2 > GO1 for PAD resistance — is the most mechanistically informative observation. The short oxa-spacer of GO1 distorts the Val21 scissile-bond geometry sufficiently to impede PR3 catalysis, while the longer spacer of GO2 accommodates a productive substrate conformation. PAD enzymes catalyze hydrolytic deimination of the guanidinium group with active-site geometry optimized for the natural Arg side chain [9]; the longer GO2 spacer introduces enough steric bulk that productive PAD engagement is impeded, while the shorter GO1 spacer is partially compatible. The inverted ranking implies that an optimal therapeutic analog may benefit from position-specific combinations of oxa-spacer lengths (GO1 at some Arg positions and GO2 at others), a hypothesis we plan to test in future combinatorial libraries.

4.4. DNA Binding: Coherence and Caveats

All DAPEG analogs retain DNA-binding capacity by qualitative gel-shift and AFM criteria. DLS reveals a quantitative gradient not captured by qualitative assays: arginine-substituted analogs form compact complexes resembling those of native LL-37, while Dap(O1)$^{[8,10,12,15,18,25]}$LL-37 and Dap(O2)$^{[8,10,12,15,18,25]}$LL-37 form considerably larger, less-condensed assemblies. This is mechanistically coherent with their reduced cationic helix face. The failure of MST to yield

 doi:10.20944/preprints202606.0060.v1

reproducible K*d* values is a methodological limitation that prevents direct ranking of binding affinities; complementary techniques (ITC, BLI, fluorescence anisotropy) are required.

A speculative pharmacological implication of the lysine-substituted profile — DNA-binding with reduced complex compaction, no antibacterial activity, full biocompatibility, suppression of degranulation — is a potential "binding without productive pro-inflammatory signaling" phenotype that could, in principle, be useful for sequestering self-DNA in autoimmune disease without amplifying inflammation [10,11,30]. Direct testing using TLR9 reporter assays in primary plasmacytoid dendritic cells will be required to substantiate this hypothesis.

4.5. Selectivity and Biocompatibility

The absence of cytotoxicity at therapeutically relevant concentrations (1–10 μM) across all tested cell lines is notable. Hydrocarbon-stapled and hypercationic LL-37 derivatives frequently show elevated hemolytic activity [12,16]; the full non-toxicity of lysine-substituted analogs up to 50 μM reflects their reduced cationicity and reduced non-specific membrane interactions [5,6,12]. The selective toxicity of all compounds against CRL-1472 bladder carcinoma at 50 μM but not against normal HB2 or HDFa cells is consistent with the documented preferential activity of LL-37 toward anionic-lipid-enriched tumor membranes [15]. The increase in differentiated HL-60 viability observed for LL-37 and the arginine-substituted analogs (Table 5) aligns with the anti-apoptotic effect of LL-37 on neutrophils through PI3K/Akt signaling downstream of FPR2 engagement [8].

4.6. The Principal Finding: Concordant Suppression of PR3 and MPO Degranulation by Lysine-Substituted Analogs

The defining pharmacological finding of this study is the dramatic, concordant suppression of LPS-induced PR3 and MPO secretion by Dap(O1)[8,10,12,15,18,25]LL-37 and Dap(O2)[8,10,12,15,18,25]LL-37 in differentiated HL-60 cells. The two-marker design was deliberately introduced to discriminate between genuine inhibition of degranulation and assay-specific artefacts: PR3 and MPO are co-stored in azurophilic primary granules but are detected through mechanistically independent assays (synthetic fluorogenic peptide substrate vs intrinsic peroxidase activity) [27–29]. Concordance between the two readouts therefore provides strong evidence for a true effect on the regulated release of granule contents. Methodological validation using the selective PR3 inhibitor (Figure 5; light-coloured bars in each panel) confirmed that the fluorescent signal reflects bona fide PR3 active-site catalysis and not artifactual fluorescence, further strengthening the interpretation of the suppression phenotype. The magnitude of the effect is striking: LPS-induced MPO secretion is reduced by ~37-fold at 1 h and by 23-fold (Dap(O1)) to 142-fold (Dap(O2)) at 24 h relative to LL-37 + LPS, with all comparisons reaching $p < 0.001$ by Sidak post-hoc and a two-way ANOVA compound F-statistic of 482.6. The residual MPO activity in analog + LPS conditions is comparable to that of unstimulated HL-60 controls, indicating near-complete inhibition of LPS-driven azurophilic granule release.

Several mechanistic hypotheses are consistent with this two-marker concordance and the structural features of the lysine-substituted analogs. First, the reduced helicity and net charge of Dap(O1)[8,10,12,15,18,25]LL-37 and Dap(O2)[8,10,12,15,18,25]LL-37 may prevent productive FPR2 engagement that drives the activating signal, while permitting partial agonism or biased signaling that suppresses TLR4 downstream pathways [7,8,22,23]. Second, these analogs may sequester LPS directly, blocking productive TLR4 receptor engagement — a known property of LL-37 itself at high doses [22,23]. Third, the analogs may engage FPR2 but with kinetically distinct receptor occupancy that produces a suppressive rather than activating downstream cascade. Discriminating among these mechanisms will require direct FPR2 binding studies, LPS-binding assays, and ideally validation in primary human neutrophils with additional readouts including reactive oxygen species generation and NET formation.

The intermediate phenotype of isoleucine-substituted Dap(MO1)[13,20,24]LL-37 and Dap(MO2)[13,20,24]LL-37 — partial suppression rather than full inhibition — likely reflects their intermediate structural properties: modestly reduced helicity but full cationic charge from preserved

 doi:10.20944/preprints202606.0060.v1

Arg and Lys residues. The dose–response position of MO analogs between the activating GO/Arg-substituted family and the suppressive O/Lys-substituted family confirms that immunomodulatory phenotype is structurally tunable within the DAPEG framework.

4.7. Limitations and Future Directions

Several limitations of this work merit explicit acknowledgement. First, proteolytic stability assays used a single isolated enzyme (PR3); stability in human serum, wound fluid or homogenates of activated neutrophils would more directly reflect translational relevance. Second, the antibacterial assays used three reference strains under standard CLSI broth-microdilution conditions; the uniform inactivity at 64 μM makes recovery of microbicidal function under physiological conditions unlikely, but cannot be formally excluded. Third, the HL-60 differentiation model is a surrogate for primary neutrophils; validation in freshly isolated human peripheral blood neutrophils — with assessment of ROS burst, NET formation and chemotactic response in addition to the two granule markers reported here — will be essential to confirm functional translation. Fourth, MST failure to yield reliable K*d* values leaves the quantitative DNA-binding ranking unresolved; complementary techniques are required. Fifth, the mechanism of anti-inflammatory action of Dap(O1)[8,10,12,15,18,25]LL-37 and Dap(O2)[8,10,12,15,18,25]LL-37 remains hypothetical; direct experimental discrimination among the alternatives listed in Section 4.6 is required. Sixth, the HL-60 degranulation assays were performed at a single peptide concentration (5.05 μM); concentration-response data for the lead Lys-substituted analogs will be required to establish IC50 values and to define a therapeutic window. Future work will address these limitations and explore combinatorial DAPEG analogs bearing position-specific oxa-spacer lengths to simultaneously optimize PR3 and PAD resistance.

5. Conclusions

We have demonstrated that the DAPEG framework provides a modular platform for cathelicidin engineering. Six analogs of LL-37 with substitutions at all Arg, all Lys or all Ile positions were obtained by Fmoc SPPS with confirmed mass, purity and partial retention of α-helical secondary structure. Substitution of arginines with a one-oxa-unit DAPEG block (Dap(GO1)[7,19,23,29,34]LL-37) yields a 5.7-fold increase in proteolytic half-life against proteinase 3; substitution with the two-oxa-unit block (Dap(GO2)[7,19,23,29,34]LL-37) confers the greatest resistance to PAD2- and PAD4-mediated citrullination but with reduced PR3 protection, establishing a position- and target-specific dependence on spacer length. All analogs retain DNA-binding capacity by qualitative assays. All six DAPEG analogs have lost direct antibacterial activity against tested reference strains, indicating that the modifications reprofile the LL-37 scaffold from microbicidal toward selective immunomodulatory function.

The principal pharmacologically novel finding is that the lysine-substituted Dap(O1)[8,10,12,15,18,25]LL-37 and Dap(O2)[8,10,12,15,18,25]LL-37 demonstrably reduce LPS-induced secretion of both proteinase 3 and myeloperoxidase from differentiated HL-60 cells — with MPO suppression reaching ~37-fold at 1 h and 23- to 142-fold at 24 h relative to LL-37 + LPS (all $p < 0.001$ by Sidak post-hoc; two-way ANOVA compound $F(7,32) = 482.6$, $p < 0.0001$) — a concordant two-marker signature that confirms genuine inhibition of azurophilic granule release, rather than enzyme-specific artefact. The isoleucine-substituted Dap(MO1)[13,20,24]LL-37 and Dap(MO2)[13,20,24]LL-37 analogs display intermediate but statistically significant partial suppression of LPS-induced MPO secretion (both Sidak $p < 0.001$ vs LL-37 + LPS at 24 h), while the arginine-substituted analogs exhibit a biphasic phenotype — activating degranulation at 1 h comparably to native LL-37 but significantly reducing MPO secretion relative to LL-37 + LPS at 24 h ($p < 0.05$ by Sidak post-hoc). The lysine-substituted DAPEG analogs therefore emerge as the most promising lead compounds from this study for further characterization in primary human neutrophils and in disease-relevant in vivo models: non-cytotoxic, with retained DNA-binding activity and protease stability, and with a concordant two-marker anti-inflammatory profile in the HL-60 surrogate model. Future work will validate these

 doi:10.20944/preprints202606.0060.v1

findings in primary human neutrophils and elucidate the mechanism through direct FPR2 binding, LPS-sequestration assays and TLR signaling experiments.

Supplementary Materials: The following supporting information can be downloaded at the website of this paper posted on Preprints.org: Section S1 — Cell culture media composition; Table S1 — Numerical MIC values for native LL-37 against reference strains; Table S2 — Raw MTT viability data (mean ± SD %) and IC50 estimates for all compounds × cell lines × concentrations; Table S3 — Raw degranulation data (PR3 and MPO, mean ± SD per condition) underlying Figures 5 and 6; Table S4 — Quantitative deconvolution of circular dichroism spectra (percentage α-helix per analog by BeStSel algorithm).

Author Contributions: Conceptualization, W.R., M.W., W.K. and A.L.; methodology, W.R., K.B., M.B., W.K. and M.W.; investigation, W.R., K.B. and M.B.; formal analysis, W.R. and M.B.; resources, M.W., W.K. and A.L.; data curation, W.R. and M.B.; writing—original draft preparation, W.R.; writing—review and editing, M.W., W.K. and A.L.; visualization, W.R.; supervision, M.W., W.K. and A.L.; project administration, A.L.; funding acquisition, A.L. and W.R. All authors have read and agreed to the published version of the manuscript.

Funding: This research was funded by the National Science Centre, Poland, grant PRELUDIUM BIS 1, number 2019/35/O/ST4/01142.

Institutional Review Board Statement: Not applicable. This study did not involve human participants or animal experiments; all biological work was performed on commercially obtained, authenticated cell lines.

Informed Consent Statement: Not applicable.

Data Availability Statement: The numerical data underlying all figures and tables in this manuscript are provided in the Supplementary Information (Tables S1–S4). Raw LC-MS spectra, mass spectrometry files, and microscopy image stacks are available from the corresponding author on reasonable request.

Acknowledgments: The authors thank Dr B. Szafranek (Physicochemical Measurements Laboratory, Faculty of Chemistry, University of Gdańsk) for assistance with DLS and zeta potential measurements, and K. Sikora MSc (Physicochemical Measurements Laboratory) for LC-MS analyses.

Conflicts of Interest: The authors declare no conflicts of interest. The funders had no role in the design of the study; in the collection, analyses, or interpretation of data; in the writing of the manuscript; or in the decision to publish the results.

Abbreviations

The following abbreviations are used in this manuscript: AMP — antimicrobial peptide; AFM — atomic force microscopy; ANOVA — analysis of variance; CD — circular dichroism; CFU — colony-forming units; CLSI — Clinical and Laboratory Standards Institute; DAPEG — diaminopropionic acid–oxa-acid framework; DLS — dynamic light scattering; DNP — 2,4-dinitrophenyl; Fmoc — 9-fluorenylmethoxycarbonyl; FPR2 — formyl peptide receptor 2; FRET — Förster resonance energy transfer; HL-60 — human promyelocytic leukemia cell line; IQF — internally quenched fluorescent; LPS — lipopolysaccharide; MALDI-TOF — matrix-assisted laser desorption/ionization time-of-flight; MIC — minimum inhibitory concentration; MPO — myeloperoxidase; MST — microscale thermophoresis; MTT — 3-(4,5-dimethylthiazol-2-yl)-2,5-diphenyltetrazolium bromide; NET — neutrophil extracellular trap; PAD — peptidylarginine deiminase; PR3 — proteinase 3; SAR — structure–activity relationship; SD — standard deviation; SPPS — solid-phase peptide synthesis; TFE — 2,2,2-trifluoroethanol; TLR — toll-like receptor; UPLC — ultra-performance liquid chromatography.

References

1. Zanetti, M. Cathelicidins, multifunctional peptides of the innate immunity. J. Leukoc. Biol. 2004, 75, 39–48. https://doi.org/10.1189/jlb.0403147.

 doi:10.20944/preprints202606.0060.v1

2. Sørensen, O.E.; Follin, P.; Johnsen, A.H.; Calafat, J.; Tjabringa, G.S.; Hiemstra, P.S.; Borregaard, N. Human cathelicidin, hCAP-18, is processed to the antimicrobial peptide LL-37 by extracellular cleavage with proteinase 3. Blood 2001, 97, 3951–3959. https://doi.org/10.1182/blood.V97.12.3951.
3. Wang, G. Structures of human host defense cathelicidin LL-37 and its smallest antimicrobial peptide KR-12 in lipid micelles. J. Biol. Chem. 2008, 283, 32637–32643. https://doi.org/10.1074/jbc.M805533200.
4. Henzler-Wildman, K.A.; Martinez, G.V.; Brown, M.F.; Ramamoorthy, A. Perturbation of the hydrophobic core of lipid bilayers by the human antimicrobial peptide LL-37. Biochemistry 2004, 43, 8459–8469. https://doi.org/10.1021/bi036284s.
5. Johansson, J.; Gudmundsson, G.H.; Rottenberg, M.E.; Berndt, K.D.; Agerberth, B. Conformation-dependent antibacterial activity of the naturally occurring human peptide LL-37. J. Biol. Chem. 1998, 273, 3718–3724. https://doi.org/10.1074/jbc.273.6.3718.
6. Oren, Z.; Lerman, J.C.; Gudmundsson, G.H.; Agerberth, B.; Shai, Y. Structure and organization of the human antimicrobial peptide LL-37 in phospholipid membranes. Biochem. J. 1999, 341, 501–513. https://doi.org/10.1042/0264-6021:3410501.
7. De Yang; Chen, Q.; Schmidt, A.P.; Anderson, G.M.; Wang, J.M.; Wooters, J.; Oppenheim, J.J.; Chertov, O. LL-37, the neutrophil granule- and epithelial cell-derived cathelicidin, utilizes formyl peptide receptor-like 1 (FPRL1) as a receptor to chemoattract human peripheral blood neutrophils, monocytes, and T cells. J. Exp. Med. 2000, 192, 1069–1074. https://doi.org/10.1084/jem.192.7.1069.
8. Nagaoka, I.; Tamura, H.; Hirata, M. An antimicrobial cathelicidin peptide, human CAP18/LL-37, suppresses neutrophil apoptosis via the activation of formyl-peptide receptor-like 1 and P2X7. J. Immunol. 2006, 176, 3044–3052. https://doi.org/10.4049/jimmunol.176.5.3044.
9. Papayannopoulos, V. Neutrophil extracellular traps in immunity and disease. Nat. Rev. Immunol. 2018, 18, 134–147. https://doi.org/10.1038/nri.2017.105.
10. Lande, R.; Ganguly, D.; Facchinetti, V.; Frasca, L.; Conrad, C.; Gregorio, J.; Meller, S.; Chamilos, G.; Sebasigari, R.; Riccieri, V.; et al. Neutrophils activate plasmacytoid dendritic cells by releasing self-DNA–peptide complexes in systemic lupus erythematosus. Sci. Transl. Med. 2011, 3, 73ra19. https://doi.org/10.1126/scitranslmed.3001180.
11. Takahashi, T.; Kulkarni, N.N.; Lee, E.Y.; Zarate-Garcia, P.M.; Wong, G.C.L.; Gallo, R.L. Cathelicidin promotes inflammation by enabling binding of self-RNA to cell surface scavenger receptors. Sci. Rep. 2018, 8, 4032. https://doi.org/10.1038/s41598-018-22409-3.
12. Wang, G.; Hanke, M.L.; Mishra, B.; Lushnikova, T.; Heim, C.E.; Chittezham Thomas, V.; Bayles, K.W.; Kielian, T. Transformation of human cathelicidin LL-37 into selective, stable, and potent antimicrobial compounds. ACS Chem. Biol. 2014, 9, 1997–2002. https://doi.org/10.1021/cb500475y.
13. Nijnik, A.; Hancock, R.E.W. Host defense peptides: antimicrobial and immunomodulatory activity and potential applications for tackling antibiotic-resistant infections. Emerg. Health Threats J. 2009, 2, e1. https://doi.org/10.3134/ehtj.09.001.
14. de Breij, A.; Riool, M.; Cordfunke, R.A.; Malanovic, N.; de Boer, L.; Koning, R.I.; Ravensbergen, E.; Franken, M.; van der Heijde, T.; Boekema, B.K.; et al. The antimicrobial peptide SAAP-148 combats drug-resistant bacteria and biofilms. Sci. Transl. Med. 2018, 10, eaan4044. https://doi.org/10.1126/scitranslmed.aan4044.
15. Xhindoli, D.; Pacor, S.; Benincasa, M.; Scocchi, M.; Gennaro, R.; Tossi, A. The human cathelicidin LL-37 — a pore-forming antibacterial peptide and host-cell modulator. Biochim. Biophys. Acta 2016, 1858, 546–566. https://doi.org/10.1016/j.bbamem.2015.11.003.
16. Walensky, L.D.; Bird, G.H. Hydrocarbon-stapled peptides: principles, practice, and progress. J. Med. Chem. 2014, 57, 6275–6288. https://doi.org/10.1021/jm4011675.
17. Molchanova, N.; Hansen, P.R.; Franzyk, H. Advances in development of antimicrobial peptidomimetics as potential drugs. Molecules 2017, 22, 1430. https://doi.org/10.3390/molecules22091430.
18. Wysocka, M.; Gruba, N.; Grzywa, R.; Giełdoń, A.; Bąchor, R.; Brzozowski, K.; Sieńczyk, M.; Jenne, D.; Szewczuk, Z.; Rolka, K.; et al. PEGylated substrates of NSP4 protease: A tool to study protease specificity. Sci. Rep. 2016, 6, 22856. https://doi.org/10.1038/srep22856.

 doi:10.20944/preprints202606.0060.v1

19. Wysocka, M.; Romanowska, A.; Gruba, N.; Michalska, M.; Giełdoń, A.; Bąchor, R.; Szewczuk, Z.; Lesner, A. A peptidomimetic fluorescent probe to detect the trypsin β2 subunit of the human 20S proteasome. Int. J. Mol. Sci. 2020, 21, 2396. https://doi.org/10.3390/ijms21072396.
20. Romanowska, A.; Rachubik, P.; Piwkowska, A.; Wysocka, M. Polymers of functionalized diaminopropionic acid are efficient mediators of active exogenous enzyme delivery into cells. Sci. Rep. 2024, 14, 13185. https://doi.org/10.1038/s41598-024-63897-w.
21. Mallek, W.; Romanowska, A.; Machowicz, W.; Piwkowska, A.; Lesner, A.; Wysocka, M. Lipidated DAPEG polymers as a non-toxic transfection agent — influence of fatty acid side chain on transfection efficacy. Molecules 2025, 30, 1644. https://doi.org/10.3390/molecules30071644.
22. Mookherjee, N.; Brown, K.L.; Bowdish, D.M.E.; Doria, S.; Falsafi, R.; Hokamp, K.; Roche, F.M.; Mu, R.; Doho, G.H.; Pistolic, J.; et al. Modulation of the TLR-mediated inflammatory response by the endogenous human host defense peptide LL-37. J. Immunol. 2006, 176, 2455–2464. https://doi.org/10.4049/jimmunol.176.4.2455.
23. Scott, M.G.; Davidson, D.J.; Gold, M.R.; Bowdish, D.; Hancock, R.E.W. The human antimicrobial peptide LL-37 is a multifunctional modulator of innate immune responses. J. Immunol. 2002, 169, 3883–3891. https://doi.org/10.4049/jimmunol.169.7.3883.
24. Neumann, A.; Völlger, L.; Berends, E.T.M.; Molhoek, E.M.; Stapels, D.A.C.; Midon, M.; Friães, A.; Pingoud, A.; Rooijakkers, S.H.M.; Gallo, R.L.; et al. Novel role of the antimicrobial peptide LL-37 in the protection of neutrophil extracellular traps against degradation by bacterial nucleases. J. Innate Immun. 2014, 6, 860–868. https://doi.org/10.1159/000363699.
25. Hancock, R.E.W.; Sahl, H.G. Antimicrobial and host-defense peptides as new anti-infective therapeutic strategies. Nat. Biotechnol. 2006, 24, 1551–1557. https://doi.org/10.1038/nbt1267.
26. Zielke, C.; Nielsen, J.E.; Lin, J.S.; Barron, A.E. Between good and evil: Complexation of the human cathelicidin LL-37 with nucleic acids. J. Biol. Chem. 2024, 300, 107878. https://doi.org/10.1016/j.jbc.2024.107878.
27. Klebanoff, S.J. Myeloperoxidase: friend and foe. J. Leukoc. Biol. 2005, 77, 598–625. https://doi.org/10.1189/jlb.1204697.
28. Faurschou, M.; Borregaard, N. Neutrophil granules and secretory vesicles in inflammation. Microbes Infect. 2003, 5, 1317–1327. https://doi.org/10.1016/j.micinf.2003.09.008.
29. Aratani, Y. Myeloperoxidase: its role for host defense, inflammation, and neutrophil function. Arch. Biochem. Biophys. 2018, 640, 47–52. https://doi.org/10.1016/j.abb.2018.01.004.
30. Kahlenberg, J.M.; Kaplan, M.J. Little peptide, big effects: the role of LL-37 in inflammation and autoimmune disease. J. Immunol. 2013, 191, 4895–4901. https://doi.org/10.4049/jimmunol.1302005.
31. Bowdish, D.M.E.; Davidson, D.J.; Hancock, R.E.W. A re-evaluation of the role of host defense peptides in mammalian immunity. Curr. Protein Pept. Sci. 2005, 6, 35–51. https://doi.org/10.2174/1389203053027494.